Published in final edited form as:
Mol Microbiol. 2014 February ; 91(3): 438–451. doi:10.1111/mmi.12470.

Sphingolipid signaling mediates mitochondrial dysfunctions and reduced chronological lifespan in the yeast model of Niemann-Pick type C1

Rita Vilaça[1,2], **Elísio Silva**[1,2], **André Nadais**[1,2], **Vítor Teixeira**[1,2], **Nabil Matmati**[3], **Joana Gaifem**[1], **Yusuf A. Hannun**[3], **Maria Clara Sá Miranda**[1], and **Vítor Costa**[1,2,*]

[1]IBMC, Instituto de Biologia Molecular e Celular, Universidade do Porto, Rua do Campo Alegre, 823, 4150-180 Porto, Portugal

[2]ICBAS, Instituto de Ciências Biomédicas Abel Salazar, Departamento de Biologia Molecular, Universidade do Porto, Rua de Jorge Viterbo Ferreira, 228, 4050-313 Porto, Portugal

[3]Stony Brook Cancer Center, Stony Brook University, Health Science Center, Stony Brook, NY, USA

Summary

The Niemann-Pick type C is a rare metabolic disease with a severe neurodegenerative phenotype characterized by an accumulation of high amounts of lipids (cholesterol and sphingolipids) in the late endosomal/lysosomal network. It is caused by loss-of-function point mutations in either NPC1 or NPC2, which seem to mediate proper intracellular lipid transport through endocytic pathway. In this study, we show that yeast cells lacking Ncr1p, an orthologue of mammalian NPC1, exhibited a higher sensitivity to hydrogen peroxide and a shortened chronological lifespan. These phenotypes were associated with increased levels of oxidative stress markers, decreased levels of antioxidant defenses and mitochondrial dysfunctions. Moreover, we report that Ncr1p deficient cells displayed high levels of long chain bases (LCB), and that Sch9p-phospho-T570 and Sch9p levels increased in *ncr1*Δ cells through a mechanism regulated by Pkh1p, a LCB-activated protein kinase. Notably, deletion of *PKH1* or *SCH9* suppressed *ncr1*Δ phenotypes but downregulation of de novo sphingolipid biosynthesis had no protective effect, suggesting that LCBs accumulation may result from an increased turnover of complex sphingolipids. These results suggest that sphingolipid signaling through Pkh1p-Sch9p mediate mitochondrial dysfunction, oxidative stress sensitivity and shortened chronological lifespan in the yeast model of Niemann-Pick type C disease.

Keywords

Niemann-Pick type C; sphingolipid signaling; mitochondria; lifespan; Pkh1p; Sch9p

Introduction

Niemann-Pick type C (NPC) disease is an autosomal recessive neurodegenerative disorder, with cellular lipid trafficking defects, involving more specifically low-density-lipoprotein derived cholesterol (Pentchev *et al.*, 1994), and is characterized by progressive neurological

*Corresponding author: Vítor Costa, Instituto de Biologia Molecular e Celular, Rua do Campo Alegre, 823. 4150-180 Porto. Portugal. Phone: +351 22 6074961. Fax: +351 22 6099157. vcosta@ibmc.up.pt.

Conflict of interests
The authors have no conflict of interest to declare.

deterioration with general symptoms of splenomegaly and dementia (Vanier, 2010). Besides cholesterol sequestration, NPC cells can also accumulate other lipids such as gangliosides and sphingolipids (Vanier, 1999) including sphingosine (Lloyd-Evans *et al.*, 2008). NPC is caused by loss-of-function point mutations in either NPC1 that accounts for 95 % of the cases (Carstea *et al.*, 1997) or NPC2 (Naureckiene *et al.*, 2000). The NPC1 protein is a large transmembrane protein that is located in the transient late endosome/lysosome system, while NPC2 protein is a soluble glycoprotein with high affinity for cholesterol (Vanier & Millat, 2004, Ko *et al.*, 2003). Both proteins seem to be involved in intracellular transport of endocytosed cholesterol through the endolysosomal system (Kwon *et al.*, 2009). Since the deficiency in NPC1 or NPC2 results in similar phenotypes and cellular lesions (Walkley & Suzuki, 2004, Sleat *et al.*, 2004), it has been suggested that both proteins function sequentially in the same pathway. However, the exact function of each protein and the molecular mechanisms associated with NPC disease remain poorly characterized.

Several pieces of evidence suggest that oxidative stress is associated with NPC pathophysiology (Vazquez *et al.*, 2012). These include changes in the expression of antioxidant defenses in NPC fibroblasts (Reddy *et al.*, 2006), NPC hepatocytes (Vazquez *et al.*, 2011), and NPC1 cerebellum (Cologna *et al.*, 2012), higher levels of reactive oxygen species and accumulation of oxidized lipids (Zampieri *et al.*, 2009) and proteins (Vazquez *et al.*, 2011). Oxidative stress is tightly linked to mitochondrial dysfunction, either because mitochondria are a generator or a target of reactive oxygen species (ROS) (Murphy, 2009). NPC cells present mitochondrial dysfunctions that have been associated with the accumulation of cholesterol in mitochondria of NPC neurons and hepatocytes (Yu *et al.*, 2005, Ikonen & Holtta-Vuori, 2004, Charman *et al.*, 2010). Changes in calcium homeostasis may also contribute to mitochondrial dysfunctions, since NPC cells exhibit defects in lysosomal Ca^{2+} uptake and NAADP-mediated lysosomal Ca^{2+} release (Lloyd-Evans & Platt, 2011). It was recently shown that δ-tocopherol, a minor vitamin E species, reduces cholesterol accumulation in NPC1 cells by enhancing lysosomal exocytosis associated with an increase of intracellular calcium concentration and amelioration of lysosomal calcium deficiency (Xu *et al.*, 2012). Moreover, the accumulation of sphingomyelin in the lysosome lumen inhibits TRPML1-mediated lysosomal Ca^{2+} release, blocking Ca^{2+}-dependent membrane trafficking (Shen *et al.*, 2012).

NPC1 and NPC2 are conserved from yeast to humans (Berger *et al.*, 2005b, Berger *et al.*, 2005a) and *Saccharomyces cerevisiae* has been used as a model system to study the cellular and molecular consequences of NPC deficiency. There is 35 % amino acid sequence identity between NPC1 and Ncr1p, and the expression of Ncr1p in NPC1 deficient cells suppresses cholesterol and ganglioside accumulation (Malathi *et al.*, 2004). Moreover, both proteins reside in the membrane of the lysosomal (vacuolar in yeast)/endosomal systems (Zhang *et al.*, 2004, Berger *et al.*, 2005a). A recent study identified 12 pathways and 13 genes required for growth of Ncr1p deficient cells under anaerobiosis, a sterol auxotrophy condition, and showed that histone deacetylase inhibition corrects for cholesterol and sphingolipid transport defects in human NPC disease (Munkacsi *et al.*, 2011). Thus, yeast is a powerful model system that can be used to identify new targets for pharmacological intervention in NPC disease. A large-scale comparison of yeast deletion strains also showed that *NCR1* deleted cells exhibit a shortened chronological lifespan (Laschober *et al.*, 2010).

Sphingolipids are ubiquitous structural components of eukaryotic cell membranes and function as signaling molecules for regulating proliferation, mitogenesis, cell migration, apoptosis, cell senescence and inflammation (Hannun & Obeid, 2008). As mentioned above, the accumulation of the long chain sphingoid base (LCB) sphingosine has been implicated in NPC disease (Lloyd-Evans *et al.*, 2008). In yeast, LCB activate the Pkh1/2p protein kinases, homologues of mammalian phosphoinositide-dependent protein kinase 1 (PDK1), which

then phosphorylate a T570 residue in the activation loop of Sch9p, a homologue of mammalian ribosomal S6 kinase also related to mammalian Akt/protein kinase B (Roelants *et al.*, 2004, Liu *et al.*, 2005, Voordeckers *et al.*, 2011). *In vitro* studies suggest that Sch9p also can be activated by PHS through a Pkh1p-independent mechanism (Liu *et al*., 2005). Sch9p is also phosphorylated in the C terminus by the target of rapamycin complex 1 (TORC1; Urban *et al.*, 2007). The Sch9p kinase is involved in modulation of mitochondrial function (Lavoie & Whiteway, 2008, Pan & Shadel, 2009), entry and exit from stationary phase (Pedruzzi *et al.*, 2003, Martinez *et al.*, 2004), nutrient changes adaptation (Roosen *et al.*, 2005), redox homeostasis and chronological lifespan (Fabrizio *et al.*, 2001) although its downstream effectors are not fully characterized.

In this study, we show that *ncr1*Δ cells exhibit mitochondrial fragmentation/dysfunction, oxidative stress sensitivity and shortened CLS associated with the accumulation of LCBs. Moreover, we report that sphingolipid signaling through Pkh1p-Sch9p contributes to *ncr1*Δ phenotypes.

Results

*ncr1*Δ cells exhibit hydrogen peroxide sensitivity and shortened chronological lifespan associated with oxidative stress markers

The yeast model of NPC disease was generated by deletion of *NCR1* gene in the *S. cerevisiae* BY4741 strain. Staining of yeast cells with filipin confirmed the accumulation of high levels of intracellular ergosterol in *ncr1*Δ cells (Supplemental Fig. S1; Brett *et al.*, 2011), a cell membrane sterol found in fungi that serves the same functions as cholesterol in mammalian cells. This is consistent with the hallmark of NPC disease, namely cholesterol accumulation due to lipid trafficking defects (Pentchev *et al*., 1994).

Since oxidative stress has been associated with NPC pathophysiology (Vazquez *et al.*, 2012), we examined cellular viability, the accumulation of oxidative damages and intracellular oxidation in *S. cerevisiae* BY4741 (parental strain) and *ncr1*Δ cells grown to exponential phase and exposed to 1.5 mM H_2O_2 during 1 h. The results show that *ncr1*Δ cells were significantly more sensitive to H_2O_2 than parental cells (Fig. 1A): 9% of *ncr1*Δ cells remained viable whereas 24% of wild-type cells survived. In agreement, H_2O_2-induced oxidative stress markers were significantly higher in *ncr1*Δ cells when compared to parental cells: protein oxidation increased 7.5-fold in *ncr1*Δ cells and 4-fold in parental cells (Fig. 1B); lipid peroxidation increased 2.5-fold in *ncr1*Δ cells but no significant changes were observed in parental cells (Fig. 1C); the % of ROS positive cells was 47% for *ncr1*Δ mutants and 24% for the parental strain (Fig. 1D). Notably, basal ROS levels were 3.5-fold higher in *ncr1*Δ cells when compared to parental cells. These results suggest that Ncr1p deficiency confers a higher sensitivity to hydrogen peroxide associated with an increased accumulation of oxidative stress markers.

Oxidative stress induced by endogenous factors, such as mitochondrial dysfunctions, has been associated with the progressive loss of cellular functions and viability during aging (Longo *et al.*, 2012). Thus, we also investigated the effect of Ncr1p deficiency on yeast chronological lifespan (CLS), which is assessed by following the survival of non-dividing cells over time. This assay is a well-established cell model to study aging of post-mitotic cells (Fabrizio & Longo, 2003). Yeast cells were grown to stationary phase and kept in the growth medium over time. Cells lacking Ncr1p exhibited a shortened CLS, as shown by an accelerated loss of viability (Fig. 2A): in cells aged for 2 and 4 days, the viability of *ncr1*Δ mutants (55% and 13%, respectively) was significantly lower than that of parental cells (>93%). The premature aging and oxidative stress sensitivity of cells lacking Ncr1p were

also observed in the W303a strain background (Supplementary Fig. S2), suggesting that *ncr1*Δ phenotypes are not strain specific.

The analysis of intracellular oxidation at post-diauxic shift phase (PDS; respiration-adapted cells), using the molecular probe dihydrorhodamine 123 that becomes fluorescent upon oxidation by hydrogen peroxide (Henderson & Chappell, 1993), shows that, compared with parental cells, Ncr1p deficient cells accumulated higher levels of ROS (Fig. 2B). Consistently, *ncr1*Δ mutant cells presented higher levels of protein carbonylation and lipid peroxidation (Fig. 2C–D). Aiming to assess if the accumulation of oxidative damages in Ncr1p deficient cells was correlated with defects in antioxidant defenses, we measured the activity of superoxide dismutase and catalase, which have important roles in the elimination of superoxide radicals and H_2O_2, respectively, as well as the levels of glutathione, a major non enzymatic antioxidant defense (Farrugia & Balzan, 2012). The results show that, although total superoxide dismutase (Sod) activity was similar in parental (BY4741) and *ncr1*Δ cells (Fig. 3A), the activity of the mitochondrial Sod (Sod2p or Mn-Sod) was significantly reduced in *ncr1*Δ cells (Fig. 3C). In addition, *ncr1*Δ cells presented lower levels of cytosolic catalase T (Ctt1p) activity (Fig. 3B, D) and glutathione (Fig. 3E), which is consistent with H_2O_2 accumulation in these mutants. It is well established that yeast are able to sense reactive oxygen species and to activate transcription factors, including Yap1p, Skn7p and Msn2/4p, that enhance the expression of genes associated with antioxidant defenses (de la Torre-Ruiz *et al.*, 2010). Thus, our results suggest that Ncr1p deficiency seems to impair this adaptive response. Interestingly, the overexpression of *SOD2* or *CTT1* was not sufficient to increase chronological lifespan in *ncr1*Δ cells (Supplementary Fig. S4), suggesting that the accumulation of oxidative damages is probably a consequence rather than the cause for the premature aging of Ncr1p deficient cells.

*ncr1*Δ cells exhibit mitochondrial dysfunctions

The high levels of ROS and the lower activity of Sod2p displayed by *ncr1*Δ cells led us to postulate that this mutant presents mitochondrial dysfunctions. To test this hypothesis, we measured oxygen consumption, cytochrome *c* oxidase (COX) activity, porin levels and the capacity of the cells to grow on a non-fermentable carbon source (glycerol), which requires functional mitochondria. In parental cells, oxygen consumption rate increased during growth from exponential to PDS phase (Fig. 4A), which is consistent with the catabolic derepression and induction of mitochondrial activity associated with the transition from fermentative to respiratory metabolism (Santangelo, 2006). The COX activity was very low at the exponential phase (data not shown), being highly induced in PDS phase cells. Notably, oxygen consumption rate and COX activity were significantly lower in Ncr1p deficient cells (Fig. 4A–B) and these mutants were unable to grow on a non-fermentable (respiratory) carbon source (Fig. 4D). The levels of porin, another mitochondrial protein, decreased only 40% in *ncr1*Δ cells grown to PDS phase (Fig. 4C). These results suggest that the very low activities of COX and Sod2p may result in part from a decreased mitochondrial mass but also from the loss of function of these enzymes in *ncr1*Δ mutants. To get further insights into changes in mitochondrial function, we assessed the mitochondrial membrane potential ($\Delta\psi_m$) by labeling parental and *ncr1*Δ cells with a mitochondria-specific voltage-dependent dye, $DiOC_6(3)$, which aggregates and preferentially accumulates into functional mitochondria. When the mitochondrial membrane depolarizes, the dye no longer accumulates in mitochondria and becomes distributed throughout the cell, resulting in a decrease in green fluorescence (Rottenberg & Wu, 1998). Our results show that cells lacking Ncr1p presented a significant drop in $\Delta\psi_m$ (Fig. 4E), indicating an increase in mitochondrial depolarization. The integrity of the mitochondrial network was also assessed by fluorescence microscopy using cells expressing a mitochondria-targeted DsRed protein. The parental cells grown to the PDS phase exhibited a normal mitochondrial tubular network.

However, loss of Ncr1p led to the formation of a punctuate pattern indicative of mitochondrial network fragmentation (Fig. 4F). The overall results suggest that *ncr1*Δ mutant cells exhibit severe mitochondrial dysfunction after the PDS.

The Pkh1p-Sch9p pathway is involved in oxidative stress sensitivity, premature aging and mitochondrial dysfunctions of *ncr1*Δ cells

Lloyd-Evans *et al*. showed that, in addition to cholesterol, NPC cells accumulate sphingosine (Lloyd-Evans *et al*., 2008). This led us to postulate that similar changes in sphingolipid species occur in Ncr1p deficient cells and that sphingolipid signaling probably is associated with *ncr1*Δ phenotypes. We analyzed the levels of long chain sphingoid bases (dihydrosphingosine (DHS), phytosphingosine (PHS) and their 1-phosphate forms) in parental and *ncr1*Δ cells at the exponential (fermentative) and PDS (respiratory) phases (Fig. 5A–D).

The parental strain showed increasing levels of PHS (1.7-fold) and PHS-1-P (2.2-fold) in cells grown from exponential to PDS phase, but DHS and DHS-1-P decreased 2.4- and 4.1-fold, respectively. The deletion of *NCR1* increased the basal levels of DHS-1-P (3.9-fold) and PHS-1-P (2.6-fold) in exponential phase cells, leading to higher ratios of DHS-1-P/DHS (3.1-fold) and PHS-1-P/PHS (1.8-fold). However, in the PDS phase, *ncr1*Δ cells exhibited higher levels of DHS (2.6-fold) and PHS (1.9-fold) and a lower DHS-1-P/DHS ratio (1.8-fold), compared with parental cells. This lipidomic analysis showed that the accumulation of LCBs displayed by NPC cells (Lloyd-Evans *et al*., 2008) is conserved in yeast *ncr1*Δ cells.

LCBs are known activators of the Pkh1p and Pkh2p protein kinases (Liu *et al*., 2005) that activate the Sch9p kinase by phosphorylating a T570 residue (Roelants *et al*., 2004, Voordeckers *et al*., 2011). Thus, we postulated that accumulation of LCBs mediates *ncr1*Δ phenotypes via modulation of a Pkh1p-Sch9p cascade. To characterize changes in this pathway associated with *NCR1* deletion, the phosphorylation of Sch9p-T570 was analyzed by Western blotting. The *ncr1*Δ cells showed significantly higher levels of Sch9p-phospho-T570 (1.9-fold), concomitantly with a proportional increase of Sch9p expression (2-fold) (Fig. 6A). These results suggest that changes in Sch9p occur mainly at protein level. Nevertheless, the increase in the levels of both Sch9p and Sch9p-phospho-T570 was significantly attenuated in *ncr1*Δ*pkh1*Δ double mutants indicating that it is mediated by Pkh1p-dependent mechanisms.

Next, we assessed the effect of *PKH1* and *SCH9* disruption on *ncr1*Δ cells. The *pkh1*Δ and *sch9*Δ cells exhibited a CLS and hydrogen peroxide resistance similar or slightly higher to that of parental cells, respectively (Fig. 6B–C). Other groups reported that *SCH9* deletion significantly increases oxidative stress resistance and lifespan (Fabrizio *et al*., 2001) in contrast with the very small protective effect observed in the present study. This probably results from differences in the growth medium composition, in particular amino acid concentration. Indeed, it was recently shown that *sch9*Δ mutants exhibit an increased lifespan when cells are grown in media supplemented with a 3.5-fold excess of amino acids but have even shorter lifespan than parental cells when they are grown in media with 0.5X amino acids (Wu *et al.*, 2013). Most importantly, the hydrogen peroxide sensitivity and shortened CLS of *ncr1*Δ cells was suppressed when *PKH1* or *SCH9* were disrupted in *ncr1*Δ cells (Fig. 6B–C). The defective cell growth on glycerol plates, decreased oxygen consumption, mitochondrial depolarization and mitochondrial network fragmentation displayed by *ncr1*Δ cells were also suppressed in both *ncr1*Δ*pkh1*Δ and *ncr1*Δ*sch9*Δ double mutants (Fig. 7A–D).

It was recently shown that downregulation of sphingolipid synthesis with myriocin, an inhibitor of serine palmitoyltransferase, increases yeast CLS in part due to a reduction of the

Pkh1p-Sch9p activity (Huang *et al.*, 2012). Thus, we also investigated the effect of myriocin on the CLS of *ncr1*Δ cells. Our results show that myriocin increased the lifespan of parental cells, but not of *ncr1*Δ mutants (Fig. 6D). This suggests that LCB accumulation may result from an increased turnover of complex sphingolipids and not from de novo biosynthesis. Nevertheless, the hypothesis that LCB-independent Sch9p functions also contribute to the shortened CLS of *ncr1*Δ cells cannot be excluded.

SCH9 deletion attenuates changes in sphingolipid homeostasis of *ncr1*Δ cells

We also investigated if the suppression of *ncr1*Δ phenotypes upon *SCH9* deletion was associated with the modulation of sphingolipid homeostasis. Regarding LCBs (Fig. 5A–D), *sch9*Δ single mutants did not exhibit major changes in either exponential or PDS phase. However, the high levels of DHS and PHS exhibited by *ncr1*Δ cells grown to PDS phase were suppressed in *ncr1*Δ*sch9*Δ cells. The overall data suggests that Sch9p mediates changes in sphingolipid metabolism associated with Ncr1p deficiency.

Discussion

The NPC disease represents the most common cause of childhood neurodegeneration. It has been intensively studied in the last years, mostly because it shares key features with emerging neurodegenerative disorders such as Alzheimer and Parkinson (Liu *et al.*, 2010). Therefore, it is hoped that a comprehensive characterization of the molecular basis of lysosomal storage diseases will contribute to the understanding of the signaling pathways and regulatory mechanisms underlying these diseases, therefore opening new avenues for therapeutic interventions. The only therapeutic agent approved in Europe for NPC disease is miglustat, a reversible inhibitor of glycosphingolipid synthesis (Wraith & Imrie, 2009), which ameliorates some neurological symptoms (Pineda *et al.*, 2010).

Yeast mutants lacking Ncr1p, the yeast orthologue of mammalian NPC1, have been used as an important model system to elucidate molecular mechanisms underlying the pathophysiology of NPC disease. Ncr1p is a vacuolar membrane protein that transits through the biosynthetic vacuolar protein sorting pathway, but it does not have an essential role in endocytic transport (Berger *et al*., 2005a, Zhang *et al*., 2004). Deletion of *NCR1* leads to resistance to the ether lipid cytotoxic drug, edelfosine, which is not suppressed in *ncr1*Δ cells expressing Ncr1p carrying amino acid changes corresponding to human NPC1 patient mutations (Berger *et al*., 2005a, Zhang *et al*., 2004). Munkacsi *et al*. have recently shown that the deletion of components of the yeast NuA4 histone acetyltransferase complex in *ncr1*Δ cells confers anaerobic inviability and accumulation of multiple sterol intermediates, and that the inhibition of histone deacetylase corrects for cholesterol and sphingolipid transport defects in human NPC disease (Munkacsi *et al*., 2011). In this report we show that *ncr1*Δ cells were hypersensitive to oxidative stress induced by hydrogen peroxide, exhibiting higher levels of oxidative stress markers, namely protein carbonylation, lipid peroxidation and ROS. Similar features were observed in NPC1 cells (Zampieri *et al*., 2009) and in hepatocytes of NPC mice (Vazquez *et al*., 2011).

Resistance to oxidative stress has been correlated with longevity in numerous eukaryotic model systems, including yeast (Fabrizio & Longo, 2003, Pan, 2011). Our results show that *ncr1*Δ cells also displayed a premature aging phenotype associated with prominent changes in redox homeostasis and oxidative stress responses during the transition from fermentative to respiratory metabolism. Indeed, *ncr1*Δ cells at the PDS phase exhibited higher levels of intracellular ROS and of oxidized proteins and lipids. In addition, antioxidant defense systems were significantly compromised in *ncr1*Δ cells, namely glutathione, a low molecular weight non-protein thiol with a major role in the regulation of redox homeostasis and ROS scavenging (Costa & Moradas-Ferreira, 2001), as well as the mitochondrial

superoxide dismutase (Sod2p) and the cytosolic catalase T (Ctt1p) which catalyze the dismutation of superoxide radicals into hydrogen peroxide and the decomposition of hydrogen peroxide, respectively. The activity of Sod1p, the superoxide dismutase present in the cytosol and in the mitochondrial intermembrane space, was not affected in *ncr1*Δ cells. In contrast, it was recently shown that *SOD1* (Cu, Zn-superoxide dismutase) and *CCS* (copper chaperone for SOD1) gene expression are down regulated in hepatocytes of NPC mice (Vazquez *et al*., 2011) whereas SOD1 increases in NPC1 cerebellum (Cologna *et al*., 2012). Similarly to *ncr1*Δ yeast cells, a decrease in catalase activity was described in multiple organs of a mouse model of NPC (Schedin *et al.*, 1997) and in fibroblasts collected from patients (Zampieri *et al*., 2009). Yet, the overexpression of *SOD2* or *CTT1* did not reverse the premature aging phenotype of *ncr1*Δ cells, suggesting that the accumulation of oxidative damages in Ncr1p deficient cells is an effect rather than the cause for its shortened chronological lifespan.

Our data suggest that the increased ROS levels leading to the accumulation of oxidative damage in *ncr1*Δ cells result from mitochondrial dysfunction. Yeast *ncr1*Δ cells were unable to grow on a non-fermentable carbon source (which requires functional mitochondria) and presented a decrease in COX activity and oxygen consumption. The levels of porin were 40% lower in *ncr1*Δ cells, suggesting that mitochondrial mass decreased in the mutant strain, with this effect accounting for the reduction of COX and Sod2p activities. However, the very low activity of these enzymes suggests that other cellular changes contribute to their loss of function. Previous studies have associated NPC with an impaired homeostasis of metals such as iron and copper (Reddy *et al*., 2006, De Windt *et al.*, 2007, Vazquez *et al*., 2011, Goez *et al.*, 2011). This may explain the decreased activity of COX, Sod2p as well as Ctt1p, since all these proteins are metal-dependent enzymes, but further studies are required to test this hypothesis. Consistent with mitochondrial dysfunctions, Ncr1p deficient cells also presented fragmentation of the mitochondrial network and mitochondrial depolarization. Cholesterol accumulation within the mitochondrial membranes of NPC1 mouse brains and neurons has been implicated in fluidity changes and in the decrease of mitochondrial membrane potential and ATP production (Yu *et al*., 2005). Mitochondrial fragmentation was also recently described in a stem-cell derived neuronal model of NPC (Ordonez *et al*., 2012).

Importantly, *ncr1*Δ cells showed high levels of LCBs thereby providing evidence that the accumulation of sphingosine previously implicated in NPC (Lloyd-Evans *et al*., 2008) is conserved in the yeast model of this disease. Our findings also implicate sphingolipid signaling in *ncr1*Δ phenotypes. In yeast, LCBs function in cell signaling through activation of the Pkh1/2p protein kinases that are homologues of mammalian PDK1 (Liu *et al*., 2005). One of the Pkh1p protein targets is the Sch9p protein kinase (Roelants *et al*., 2004, Liu *et al*., 2005, Voordeckers *et al*., 2011), a homologue of mammalian ribosomal S6 kinase that controls stress responses and lifespan (Longo, 2003, Lavoie & Whiteway, 2008, Pan & Shadel, 2009). Huang *et al*. have recently shown that down-regulating sphingolipid synthesis increases yeast lifespan in part due to a reduction in Sch9p activity and proposed that Sch9p regulates lifespan by integrating nutrient signals from TOR1 with growth and stress signals from sphingolipids (Huang *et al*., 2012). We found that Sch9p-T570 phosphorylation and total Sch9p are increased in *ncr1*Δ cells in a Pkh1p dependent manner. Importantly, deletion of either *PKH1* or *SCH9* suppressed oxidative stress sensitivity, shortened CLS and the mitochondrial dysfunction of *ncr1*Δ cells. However, the inhibition of de novo sphingolipid biosynthesis by treatment with myriocin did not increase the lifespan of *ncr1*Δ cells. This observation suggests that other changes in sphingolipid metabolism, rather than increased de novo biosynthesis, may lead to the accumulation of LCBs in *ncr1*Δ cells, e.g. through sphingolipid turnover mediated by Isc1p, an homologue of mammalian neutral sphingomyelinase, and/or ceramidases (Ypc1p or Ydc1p). Alternatively, LCB-

Pkh1p-independent mechanisms may contribute to *ncr1*Δ phenotypes. Since Sch9p also can be phosphorylated in the C terminus by the target of rapamycin complex 1 (TORC1; Urban *et al*., 2007) and down-regulation of Sch9p mediates CLS extension associated with reduced TORC1 signaling (Pan & Shadel, 2009), deregulation of the TOR pathway may contribute to LCB-independent Sch9p-dependent phenotypes of *ncr1*Δ cells. How changes in sphingolipid dynamics or in TORC1 signaling contribute to *ncr1*Δ phenotypes is an important issue for future studies.

Moreover, autophagy is induced in NPC through a Beclin-1/class III PI3K complex-dependent mechanism (Pacheco *et al.*, 2007), but the autophagic flux seems to be impaired (Ishibashi *et al.*, 2009) due to the inhibition of cathepsin, a lysosomal protease, by stored lipids that leads to an impaired turnover of autolysosomes (Elrick *et al.*, 2012). Notably, autophagy activation, associated with an impaired completion of autophagy, promotes lipid accumulation in the NPC lysosome and, therefore, disease pathogenesis (Elrick *et al*., 2012). In yeast, Ncr1p-deficient cells present an acidic shift of vacuolar pH that correlates with ergosterol accumulation in these organelles (Brett *et al*., 2011), which may also compromise the activity of vacuolar proteases. It was recently shown that myriocin enhances autophagy in yeast (Liu *et al.*, 2013). Thus, the activation of autophagy by myriocin may be detrimental for *ncr1*Δ cells, preventing lifespan extension in this mutant.

The mechanisms underlying the phenotypes of *ncr1*Δ cells seem to be complex, with Sch9p also playing a role in mediating the changes in sphingolipid homeostasis measured in this mutant. Indeed, *SCH9* deletion suppressed the high levels of LCBs displayed by *ncr1*Δ cells. More studies are needed to further characterize how Sch9p functions upstream in the regulation of sphingolipid metabolism, in addition to its role downstream as an effector of sphingolipid signaling. Nevertheless, other studies showed that sphingolipid homeostasis is regulated by an intricate network of protein kinases and protein phosphatases that can be activated by sphingolipids but also control sphingolipid biosynthesis, e.g. through modulation of Orm1/2p (Roelants *et al.*, 2011, Liu *et al.*, 2012, Sun *et al.*, 2012, Shimobayashi *et al.*, 2013).

In summary, our data show that the yeast model of NPC disease exhibits oxidative stress sensitivity and a shortened CLS associated with oxidative stress markers and mitochondrial fragmentation and dysfunction. In addition, our findings suggest that sphingolipid signaling mediated by the LCB-activated protein kinase Pkh1p and its downstream target Sch9p mediate *ncr1*Δ phenotypes. These results highlight the importance of oxidative stress and loss of mitochondria functionality in NPC and further support the use of yeast as a valuable model to study molecular mechanisms underlying the pathophysiology of NPC disease.

Experimental procedures

Yeast strains and growth conditions

The *Saccharomyces cerevisiae* strains used in this work are listed in table 1. The growth media used were YPD [1 % (w/v) yeast extract, 2 % (w/v) bactopeptone, 2 % (w/v) glucose], YPG [1 % (w/v) yeast extract, 2 % (w/v) bactopeptone, 4 % (v/v) glycerol], synthetic complete (SC) drop-out medium containing 2% (w/v) glucose 0.67% yeast nitrogen base without amino acids, or minimal medium containing 2% (w/v) glucose 0.67% yeast nitrogen base without amino acids, supplemented with appropriate amino acids [0.008 % (w/v) histidine, 0.04 % (w/v) leucine, 0.008 % (w/v) tryptophan)] or nucleotides (0.008 % (w/v) uracil). Yeast cells were grown aerobically at 26 ºC in an orbital shaker (at 140 r.p.m.), with a ratio of flask volume / medium volume of 5:1, to early exponential phase (OD_{600nm}=0.6) or to post-diauxic phase (OD_{600nm}=7–9). To generate *ncr1*Δ::*KanMX4* cells, a deletion fragment containing *KanMX4* and the flanking regions of *NCR1* was amplified by

polymerase chain reaction (PCR) using genomic DNA from *S. cerevisiae* BY4741 *ncr1*Δ cells (Euroscarf, Germany). Yeast cells were transformed by electroporation, and *ncr1*Δ mutant cells were selected in YPD containing 0.4 mg geneticin mL^{-1} (Sigma). To generate *ncr1*Δ::*URA3* cells, the *KanMX4* cassette in *ncr1*Δ::*KanMX4* cells was replaced by *URA3*, using a deletion fragment containing an heterologous *URA3* cassette and the flanking regions of *KanMX4* that was amplified by PCR from pAG61 plasmid (Goldstein *et al.*, 1999). The *NCR1* gene was also disrupted in *pkh1*Δ and *sch9*Δ cells with a deletion fragment containing *URA3* and the flanking regions of *NCR1* that was amplified by PCR using genomic DNA from *ncr1*Δ::*URA3* cells. Cells were selected in minimal medium lacking uracil and the correct integration of all cassettes was confirmed by PCR. For *SOD2* and *CTT1* overexpression, a *Bam*HI fragment containing the *SOD2* gene under its promotor and a *Hin*dIII-*Bam*HI fragment containing the *CTT1* gene under its promotor were cloned into YEp352. BY4741 and *ncr1*Δ::KanMX4 cells were transformed by electroporation with YEp352 (empty vector), YEp352-*SOD2* and YEp352-*CTT1* and selected in minimal medium lacking uracil.

Oxidative stress resistance and chronological lifespan

For analysis of oxidative stress resistance, yeast cells were grown to exponential phase (OD_{600nm} = 0.6) and treated with 1.5 mM H_2O_2 for 1 hour. Chronological lifespan was assayed as previously described (Mesquita *et al.*, 2010). Briefly, overnight cultures were diluted to OD_{600nm}=0.6 and grown for 24 hours (to PDS phase) or 48h (stationary phase; considered t0 in the lifespan assay) and kept in culture media at 26 ºC. Cell viability was determined by standard dilution plate counts on YPD medium containing 1.5 % (w/v) agar. Colonies were counted after growth for 3 days at 26 ºC. Viability was expressed as a percentage of colony-forming units in relation to time 0 or to untreated cells, as indicated. To analyze the effect of myriocin on CLS, yeast cells were treated as described previously (Huang *et al.*, 2012) with minor modifications. A stock solution of 200 μg mL^{-1} myriocin (Sigma) was prepared in 95 % (v/v) ethanol. Cells were grown overnight and diluted to OD_{600nm}=0.01. Then, 600 ng mL^{-1} myriocin or ethanol (vehicle; volume identical to myriocin) was added to the cultures. Cells were grown to stationary phase and cell viability was measured as described above.

Protein carbonylation, lipid peroxidation and intracellular oxidation

Protein oxidation was determined by immunodetection of protein carbonyls as previously described (Costa *et al.*, 2002). Quantification of carbonyls was performed in a GS-800 densitometry (Bio-Rad). Lipid peroxidation was determined by quantification of thiobarbituric acid reactive substances as described (Belinha *et al.*, 2007) and expressed as nmol MDA mg^{-1} protein. Levels of intracellular H_2O_2 and superoxide anion were detected with dihydrorhodamine (DHR) 123 and dihydroethidium (DHE) (Molecular Probes, Life Technologies), respectively. 3×10^7 cells were treated with 6 μL of DHR (stock solution at 2.5 mg mL^{-1}; prepared in DMSO) and incubated for 60 minutes at 26 ºC, or with 1 μL of DHE (stock solution at 5 mM; prepared in DMSO) and incubated for 10 minutes at 26 ºC. Fluorescence of DHR-positive cells was measured on the FL-1 channel of a Becton Dickinson FACS Calibur Analytic Flow cytometer with excitation and emission settings of 488 nm and 515–545 nm, respectively, without compensation. The DHE staining was analyzed by flow cytometry with excitation and emission settings of 488 nm and ≥670 nm (FL3 channel) without compensation. The data was analyzed using the FlowJo software (Tree Star).

Glutathione levels and enzymatic activities

All the procedures were carried out at 4 ºC. Yeast cells were harvested by centrifugation. Glutathione levels were measured by the method of Tietze (1969), as described (Belinha *et al.*, 2007), and expressed as μmol glutathione (mg protein) $^{-1}$. For enzyme activities, yeast extracts were prepared in 50 mM potassium phosphate buffer (pH 7.0) containing protease inhibitors (Complete, Mini, EDTA-free Protease Cocktail Inhibitor Tablets; Roche Applied Science), as described (Almeida *et al.*, 2008). The activity of catalase and SOD was determined spectrophotometrically (Aebi, 1984) (Beauchamp & Fridovich, 1971) or analyzed in situ, after separation of proteins (60 μg) by native PAGE, as described (Conyers & Kidwell, 1991, Flohe & Otting, 1984). Cytochrome *c* oxidase (COX) activity was determined as previously described (Poyton *et al.*, 1995), by measuring cytochrome *c* oxidation.

Oxygen consumption and growth in glycerol

Oxygen consumption rate was measured for 3×10^8 cells at 26 ºC in phosphate buffer using an oxygen electrode (Oxygraph, Hansatech). Data were analyzed using the Oxyg32 v2.25 software. For analysis of respiratory capacity, yeast cells were grown to exponential phase (OD_{600nm} = 0.6), diluted to an OD_{600nm} = 0.1 and five-fold serial dilutions were plated in solid media containing glucose or glycerol as carbon source (YPD or YPG media supplemented with 1.5% (w/v) agar).

Mitochondrial fragmentation and mitochondrial membrane potential

Mitochondrial morphology was analyzed in cells transformed with a plasmid expressing mitochondrial DsRed (pYX222-mtDsRed). Cells were grown in SC-glucose medium lacking histidine to post-diauxic shift phase. The mitochondrial network was observed in live cells by fluorescence microscopy (AxioImager Z1, Carl Zeiss). Data image stacks were deconvolved by QMLE algorithm of Huygens Professional v3.0.2p1 (Scientific Volume Imaging B.V.). Maximum intensity projection was used to output final images using ImageJ 1.47n software. The mitochondrial membrane potential was measured by flow cytometry using cells probed with the potential-sensitive dye 3,3-dihexyloxacarbocyanine iodide [($DiOC_6(3)$], as described (Rottenberg & Wu, 1998). Briefly, 2×10^6 cells were re-suspended in suspension buffer [10 mM 2-(N-morpholino)ethanesulfonic acid (MES), 0.1 mM $MgCl_2$ and 2 % (w/v) Glucose, pH 6.0] and $DiOC_6(3)$ (Invitrogen) was added to a final concentration of 1 nM. The cell suspension was then incubated for 30 minutes at 30 ºC and washed twice with PBS. The mitochondrial membrane potential was analyzed by flow cytometry (Becton-Dickinson FACS Calibur Analytic Flow Cytometer) on the FL1-channel with excitation and emission settings of 488 nm and 525 nm, respectively. The data was analyzed using the FlowJo software (Tree Star).

Sphingolipid analysis by HPLC-MS/MS

Yeast cells were grown in SC-glucose medium and 1.9×10^9 cells were collected at exponential and PDS phase. Cell pellets were re-suspended in 1ml of lipid extraction solvent: 50 % (v/v) iso-propanol, 10 % (v/v) diethyl ether, 2 % (v/v) pyridine, 25 % (v/v) ammonia. A 200 μl volume of glass beads were added into a screw cup 2 ml plastic tubes. Tubes were shaken in a bead better 5 times, 3 min on, 1 min off at 4°C. The content of the tubes was poured into a 13×100 mm glass tubes. An additional 1 ml solvent was used to wash the plastic tubes and was added into the glass tubes. The tubes containing 2 ml solvent with cells and glass beads were dried in an analytical nitrogen evaporator (N-EVAP). The dried samples were sent to the Lipidomic Core at the Medical University of South Carolina for lipid analysis. Levels of long-chain sphingoid bases and their phosphorylated forms were measured by the high-performance liquid chromatography/mass spectrometry (LC-MS/MS)

methodology as previously described (Bielawski *et al.*, 2010). Analytical results of lipids were expressed as pmol sphingolipid/ total cell number.

Protein extraction and western blotting analysis

Yeast cells were grown in SC-glucose medium to exponential or PDS phase and protein extracts were prepared as described (Huang *et al*., 2012) with minor modifications. Briefly, 9×10^8cells were collected, suspended in 200 μl of water and 200 μl of 0.2 M NaOH. Samples were vortexed and incubated at room temperature for 5 min, centrifuged and the pellet suspended in 200 μl of gel lysis buffer (50 mM Tris-HCl pH 8.8, 2 % (w/v) SDS, 10 % (v/v) glycerol, 2 mM EDTA). After heating 5 min at 95 ºC, samples were centrifuged and the protein content of the supernatant was quantified with BCA™ Protein Assay Kit (Thermo Scientific) using bovine serum albumin as a standard. Proteins (30 μg) were mixed with 1 % (v/v) β-mercaptoethanol, heated for 2 min at 95 ºC, electrophoresed on a 9 % SDS-PAGE gel and transferred for 1.5 hours onto a nitrocellulose membrane (GE Healthcare). Each membrane was blocked in TTBS (20 mM Tris, 140 mM NaCl, 0.05 % (v/v) Tween-20 pH 7.6) containing 5 % nonfat dry milk. Membranes were then incubated with the primary antibody, mouse anti-yeast porin (Por1p) antibody (1:1000, Molecular Probes), mouse anti-yeast phosphoglycerate kinase (Pgk1p) antibody (1:40000, Molecular Probes), rabbit anti-Sch9p antibody (1:1000, kindly provided by Dr Robert Dickson) or rabbit anti-P-T570-Sch9p antibody (1:10000, kindly provided by Dr Robbie Loewith), and with the secondary antibody, anti-mouse IgG-peroxidase (1:5000, Molecular probes) or anti-rabbit IgG-peroxidase (1:5000, Sigma). Immunodetection was performed by chemiluminescence, using a kit from GE Healthcare (RPN 2109).

Statistical analysis

The results obtained were represented by mean and standard deviation values of at least three independent experiments. Statistical analyses were carried out using GraphPad Prism Software v6.02 (GraphPad Software).

Supplementary Material

Refer to Web version on PubMed Central for supplementary material.

Acknowledgments

This work was financially supported by FEDER (Fundo Europeu de Desenvolvimento Regional) through the program “Programa Operacional Fatores de Competitividade-COMPETE”, and by FCT (Fundação para a Ciência e Tecnologia) through the projects FCOMP-01-0124-FEDER-022718 (Pest-C/SAU/LA0002/2011) and NORTE-07-0124-FEDER-000001, and in part by National Institutes of Health Grant GM063265 (to Y. A. H.), the Lipidomics Shared Resource, Hollings Cancer Center, Medical University of South Carolina (P30 CA138313) and the Lipidomics Core in the SC Lipidomics and Pathobiology COBRE, Department Biochemistry, MUSC (P20 RR017677). R.V. (SFRH/BD/48125/2008) and V.T. (SFRH/BD/72134/2010) were supported by FCT fellowships. We are grateful to Paula Sampaio (ALM, IBMC) for the help with fluorescence microscopy, Catarina Leitão (AFCU, IBMC) for all the help with flow cytometry analysis, Paula Ludovico (ICVS, Universidade do Minho, Portugal) for providing the pYX222-mtDsRed plasmid, and Robert Dickson (University of Kentucky College of Medicine, Lexington, Kentucky, USA) and Robbie Loewith (University of Geneva, Switzerland) for providing antibodies used in this study.

Abbreviations

CLS	chronological lifespan
COX	cytochrome *c* oxidase
DHE	dihydroethidium

DHR	dihydrorhodamine
DHS	dihydrosphingosine
DNPH	2,4-dinitrophenylhydrazine
MDA	malondialdehyde
NPC	Niemann-Pick type C
PDS	post-diauxic shift
PHS	phytosphingosine
PVDF	polyvinylidene difluoride
ROS	reactive oxygen species
SOD	superoxide dismutase
TBARS	thiobarbituric acid reactive substances

References

Aebi H. Catalase in vitro. Methods Enzymol. 1984; 105:121–126. [PubMed: 6727660]

Almeida T, Marques M, Mojzita D, Amorim MA, Silva RD, Almeida B, Rodrigues P, Ludovico P, Hohmann S, Moradas-Ferreira P, Corte-Real M, Costa V. Isc1p plays a key role in hydrogen peroxide resistance and chronological lifespan through modulation of iron levels and apoptosis. Mol Biol Cell. 2008; 19:865–876. [PubMed: 18162582]

Beauchamp C, Fridovich I. Superoxide dismutase: improved assays and an assay applicable to acrylamide gels. Anal Biochem. 1971; 44:276–287. [PubMed: 4943714]

Belinha I, Amorim MA, Rodrigues P, de Freitas V, Moradas-Ferreira P, Mateus N, Costa V. Quercetin increases oxidative stress resistance and longevity in *Saccharomyces cerevisiae*. J Agric Food Chem. 2007; 55:2446–2451. [PubMed: 17323973]

Berger AC, Hanson PK, Wylie Nichols J, Corbett AH. A yeast model system for functional analysis of the Niemann-Pick type C protein 1 homolog, Ncr1p. Traffic. 2005a; 6:907–917. [PubMed: 16138904]

Berger AC, Vanderford TH, Gernert KM, Nichols JW, Faundez V, Corbett AH. *Saccharomyces cerevisiae* Npc2p is a functionally conserved homologue of the human Niemann-Pick disease type C 2 protein, hNPC2. Eukaryot Cell. 2005b; 4:1851–1862. [PubMed: 16278452]

Bielawski J, Pierce JS, Snider J, Rembiesa B, Szulc ZM, Bielawska A. Sphingolipid analysis by high performance liquid chromatography-tandem mass spectrometry (HPLC-MS/MS). Adv Exp Med Biol. 2010; 688:46–59. [PubMed: 20919645]

Brett CL, Kallay L, Hua Z, Green R, Chyou A, Zhang Y, Graham TR, Donowitz M, Rao R. Genome-wide analysis reveals the vacuolar pH-stat of *Saccharomyces cerevisiae*. PLoS One. 2011; 6:e17619. [PubMed: 21423800]

Carstea ED, Morris JA, Coleman KG, Loftus SK, Zhang D, Cummings C, Gu J, Rosenfeld MA, Pavan WJ, Krizman DB, Nagle J, Polymeropoulos MH, Sturley SL, Ioannou YA, Higgins ME, Comly M, Cooney A, Brown A, Kaneski CR, Blanchette-Mackie EJ, Dwyer NK, Neufeld EB, Chang TY, Liscum L, Strauss JF 3rd, Ohno K, Zeigler M, Carmi R, Sokol J, Markie D, O'Neill RR, van Diggelen OP, Elleder M, Patterson MC, Brady RO, Vanier MT, Pentchev PG, Tagle DA. Niemann-Pick C1 disease gene: homology to mediators of cholesterol homeostasis. Science. 1997; 277:228–231. [PubMed: 9211849]

Charman M, Kennedy BE, Osborne N, Karten B. MLN64 mediates egress of cholesterol from endosomes to mitochondria in the absence of functional Niemann-Pick Type C1 protein. J Lipid Res. 2010; 51:1023–1034. [PubMed: 19965586]

Cologna SM, Jiang XS, Backlund PS, Cluzeau CV, Dail MK, Yanjanin NM, Siebel S, Toth CL, Jun HS, Wassif CA, Yergey AL, Porter FD. Quantitative proteomic analysis of Niemann-Pick disease,

type C1 cerebellum identifies protein biomarkers and provides pathological insight. PLoS One. 2012; 7:e47845. [PubMed: 23144710]

Conyers SM, Kidwell DA. Chromogenic substrates for horseradish peroxidase. Anal Biochem. 1991; 192:207–211. [PubMed: 2048722]

Costa V, Amorim MA, Quintanilha A, Moradas-Ferreira P. Hydrogen peroxide-induced carbonylation of key metabolic enzymes in *Saccharomyces cerevisiae*: the involvement of the oxidative stress response regulators Yap1 and Skn7. Free Radical Biology and Medicine. 2002; 33:1507–1515. [PubMed: 12446208]

Costa V, Moradas-Ferreira P. Oxidative stress and signal transduction in *Saccharomyces cerevisiae*: insights into ageing, apoptosis and diseases. Molecular Aspects of Medicine. 2001; 22:217–246. [PubMed: 11679167]

de la Torre-Ruiz MA, Mozo-Villarias A, Pujol N, Petkova MI. How budding yeast sense and transduce the oxidative stress signal and the impact in cell growth and morphogenesis. Curr Protein Pept Sci. 2010; 11:669–679. [PubMed: 21235503]

De Windt A, Rai M, Kytomaki L, Thelen KM, Lutjohann D, Bernier L, Davignon J, Soini J, Pandolfo M, Laaksonen R. Gene set enrichment analyses revealed several affected pathways in Niemann-pick disease type C fibroblasts. DNA Cell Biol. 2007; 26:665–671. [PubMed: 17683244]

Elrick MJ, Yu T, Chung C, Lieberman AP. Impaired proteolysis underlies autophagic dysfunction in Niemann-Pick type C disease. Hum Mol Genet. 2012; 21:4876–4887. [PubMed: 22872701]

Fabrizio P, Longo VD. The chronological life span of *Saccharomyces cerevisiae*. Aging Cell. 2003; 2:73–81. [PubMed: 12882320]

Fabrizio P, Pozza F, Pletcher SD, Gendron CM, Longo VD. Regulation of longevity and stress resistance by Sch9 in yeast. Science. 2001; 292:288–290. [PubMed: 11292860]

Farrugia G, Balzan R. Oxidative stress and programmed cell death in yeast. Front Oncol. 2012; 2:64. [PubMed: 22737670]

Flohe L, Otting F. Superoxide dismutase assays. Methods Enzymol. 1984; 105:93–104. [PubMed: 6328209]

Goez HR, Jacob FD, Fealey RD, Patterson MC, Ramaswamy V, Persad R, Johnson ES, Yager JY. An unusual presentation of copper metabolism disorder and a possible connection with Niemann-Pick type C. J Child Neurol. 2011; 26:518–521. [PubMed: 21273508]

Goldstein AL, Pan X, McCusker JH. Heterologous URA3MX cassettes for gene replacement in *Saccharomyces cerevisiae*. Yeast. 1999; 15:507–511. [PubMed: 10234788]

Hannun YA, Obeid LM. Principles of bioactive lipid signalling: lessons from sphingolipids. Nat Rev Mol Cell Biol. 2008; 9:139–150. [PubMed: 18216770]

Henderson LM, Chappell JB. Dihydrorhodamine 123: a fluorescent probe for superoxide generation? Eur J Biochem. 1993; 217:973–980. [PubMed: 8223655]

Huang X, Liu J, Dickson RC. Down-regulating sphingolipid synthesis increases yeast lifespan. PLoS Genet. 2012; 8:e1002493. [PubMed: 22319457]

Ikonen E, Holtta-Vuori M. Cellular pathology of Niemann-Pick type C disease. Semin Cell Dev Biol. 2004; 15:445–454. [PubMed: 15207834]

Ishibashi S, Yamazaki T, Okamoto K. Association of autophagy with cholesterol-accumulated compartments in Niemann-Pick disease type C cells. J Clin Neurosci. 2009; 16:954–959. [PubMed: 19342246]

Ko DC, Binkley J, Sidow A, Scott MP. The integrity of a cholesterol-binding pocket in Niemann-Pick C2 protein is necessary to control lysosome cholesterol levels. Proc Natl Acad Sci U S A. 2003; 100:2518–2525. [PubMed: 12591949]

Kwon HJ, Abi-Mosleh L, Wang ML, Deisenhofer J, Goldstein JL, Brown MS, Infante RE. Structure of N-terminal domain of NPC1 reveals distinct subdomains for binding and transfer of cholesterol. Cell. 2009; 137:1213–1224. [PubMed: 19563754]

Laschober GT, Ruli D, Hofer E, Muck C, Carmona-Gutierrez D, Ring J, Hutter E, Ruckenstuhl C, Micutkova L, Brunauer R, Jamnig A, Trimmel D, Herndler-Brandstetter D, Brunner S, Zenzmaier C, Sampson N, Breitenbach M, Frohlich KU, Grubeck-Loebenstein B, Berger P, Wieser M, Grillari-Voglauer R, Thallinger GG, Grillari J, Trajanoski Z, Madeo F, Lepperdinger G, Jansen-

Durr P. Identification of evolutionarily conserved genetic regulators of cellular aging. Aging Cell. 2010; 9:1084–1097. [PubMed: 20883526]

Lavoie H, Whiteway M. Increased respiration in the sch9Delta mutant is required for increasing chronological life span but not replicative life span. Eukaryot Cell. 2008; 7:1127–1135. [PubMed: 18469137]

Liu J, Huang X, Withers BR, Blalock E, Liu K, Dickson RC. Reducing sphingolipid synthesis orchestrates global changes to extend yeast lifespan. Aging Cell. 2013; 12:833–841. [PubMed: 23725375]

Liu JP, Tang Y, Zhou S, Toh BH, McLean C, Li H. Cholesterol involvement in the pathogenesis of neurodegenerative diseases. Mol Cell Neurosci. 2010; 43:33–42. [PubMed: 19660552]

Liu K, Zhang X, Lester RL, Dickson RC. The sphingoid long chain base phytosphingosine activates AGC-type protein kinases in *Saccharomyces cerevisiae* including Ypk1, Ypk2, and Sch9. J Biol Chem. 2005; 280:22679–22687. [PubMed: 15840588]

Liu M, Huang C, Polu SR, Schneiter R, Chang A. Regulation of sphingolipid synthesis through Orm1 and Orm2 in yeast. J Cell Sci. 2012; 125:2428–2435. [PubMed: 22328531]

Lloyd-Evans E, Morgan AJ, He X, Smith DA, Elliot-Smith E, Sillence DJ, Churchill GC, Schuchman EH, Galione A, Platt FM. Niemann-Pick disease type C1 is a sphingosine storage disease that causes deregulation of lysosomal calcium. Nat Med. 2008; 14:1247–1255. [PubMed: 18953351]

Lloyd-Evans E, Platt FM. Lysosomal Ca (2+) homeostasis: role in pathogenesis of lysosomal storage diseases. Cell Calcium. 2011; 50:200–205. [PubMed: 21724254]

Longo VD. The Ras and Sch9 pathways regulate stress resistance and longevity. Exp Gerontol. 2003; 38:807–811. [PubMed: 12855292]

Longo VD, Shadel GS, Kaeberlein M, Kennedy B. Replicative and chronological aging in *Saccharomyces cerevisiae*. Cell Metab. 2012; 16:18–31. [PubMed: 22768836]

Malathi K, Higaki K, Tinkelenberg AH, Balderes DA, Almanzar-Paramio D, Wilcox LJ, Erdeniz N, Redican F, Padamsee M, Liu Y, Khan S, Alcantara F, Carstea ED, Morris JA, Sturley SL. Mutagenesis of the putative sterol-sensing domain of yeast Niemann Pick C-related protein reveals a primordial role in subcellular sphingolipid distribution. J Cell Biol. 2004; 164:547–556. [PubMed: 14970192]

Martinez MJ, Roy S, Archuletta AB, Wentzell PD, Anna-Arriola SS, Rodriguez AL, Aragon AD, Quinones GA, Allen C, Werner-Washburne M. Genomic analysis of stationary-phase and exit in *Saccharomyces cerevisiae*: gene expression and identification of novel essential genes. Mol Biol Cell. 2004; 15:5295–5305. [PubMed: 15456898]

Mesquita A, Weinberger M, Silva A, Sampaio-Marques B, Almeida B, Leao C, Costa V, Rodrigues F, Burhans WC, Ludovico P. Caloric restriction or catalase inactivation extends yeast chronological lifespan by inducing H_2O_2 and superoxide dismutase activity. Proc Natl Acad Sci U S A. 2010; 107:15123–15128. [PubMed: 20696905]

Munkacsi AB, Chen FW, Brinkman MA, Higaki K, Gutierrez GD, Chaudhari J, Layer JV, Tong A, Bard M, Boone C, Ioannou YA, Sturley SL. An “exacerbate-reverse” strategy in yeast identifies histone deacetylase inhibition as a correction for cholesterol and sphingolipid transport defects in human Niemann-Pick type C disease. J Biol Chem. 2011; 286:23842–23851. [PubMed: 21489983]

Murphy MP. How mitochondria produce reactive oxygen species. Biochem J. 2009; 417:1–13. [PubMed: 19061483]

Naureckiene S, Sleat DE, Lackland H, Fensom A, Vanier MT, Wattiaux R, Jadot M, Lobel P. Identification of HE1 as the second gene of Niemann-Pick C disease. Science. 2000; 290:2298–2301. [PubMed: 11125141]

Ordonez MP, Roberts EA, Kidwell CU, Yuan SH, Plaisted WC, Goldstein LS. Disruption and therapeutic rescue of autophagy in a human neuronal model of Niemann Pick type C1. Hum Mol Genet. 2012; 21:2651–2662. [PubMed: 22437840]

Pacheco CD, Kunkel R, Lieberman AP. Autophagy in Niemann-Pick C disease is dependent upon Beclin-1 and responsive to lipid trafficking defects. Hum Mol Genet. 2007; 16:1495–1503. [PubMed: 17468177]

Pan Y. Mitochondria, reactive oxygen species, and chronological aging: a message from yeast. Exp Gerontol. 2011; 46:847–852. [PubMed: 21884780]

Pan Y, Shadel GS. Extension of chronological life span by reduced TOR signaling requires down-regulation of Sch9p and involves increased mitochondrial OXPHOS complex density. Aging (Albany NY). 2009; 1:131–145. [PubMed: 20157595]

Pedruzzi I, Dubouloz F, Cameroni E, Wanke V, Roosen J, Winderickx J, De Virgilio C. TOR and PKA signaling pathways converge on the protein kinase Rim15 to control entry into G0. Mol Cell. 2003; 12:1607–1613. [PubMed: 14690612]

Pentchev PG, Brady RO, Blanchette-Mackie EJ, Vanier MT, Carstea ED, Parker CC, Goldin E, Roff CF. The Niemann-Pick C lesion and its relationship to the intracellular distribution and utilization of LDL cholesterol. Biochim Biophys Acta. 1994; 1225:235–243. [PubMed: 8312368]

Pineda M, Perez-Poyato MS, O'Callaghan M, Vilaseca MA, Pocovi M, Domingo R, Portal LR, Perez AV, Temudo T, Gaspar A, Penas JJ, Roldan S, Fumero LM, de la Barca OB, Silva MT, Macias-Vidal J, Coll MJ. Clinical experience with miglustat therapy in pediatric patients with Niemann-Pick disease type C: a case series. Mol Genet Metab. 2010; 99:358–366. [PubMed: 20056559]

Poyton RO, Goehring B, Droste M, Sevarino KA, Allen LA, Zhao XJ. Cytochrome-c oxidase from *Saccharomyces cerevisiae*. Methods Enzymol. 1995; 260:97–116. [PubMed: 8592475]

Reddy JV I, Ganley G, Pfeffer SR. Clues to neuro-degeneration in Niemann-Pick Type C disease from global gene expression profiling. PLoS One. 2006; 1:e19. [PubMed: 17183645]

Roelants FM, Breslow DK, Muir A, Weissman JS, Thorner J. Protein kinase Ypk1 phosphorylates regulatory proteins Orm1 and Orm2 to control sphingolipid homeostasis in *Saccharomyces cerevisiae*. Proc Natl Acad Sci U S A. 2011; 108:19222–19227. [PubMed: 22080611]

Roelants FM, Torrance PD, Thorner J. Differential roles of PDK1- and PDK2-phosphorylation sites in the yeast AGC kinases Ypk1, Pkc1 and Sch9. Microbiology. 2004; 150:3289–3304. [PubMed: 15470109]

Roosen J, Engelen K, Marchal K, Mathys J, Griffioen G, Cameroni E, Thevelein JM, De Virgilio C, De Moor B, Winderickx J. PKA and Sch9 control a molecular switch important for the proper adaptation to nutrient availability. Mol Microbiol. 2005; 55:862–880. [PubMed: 15661010]

Rottenberg H, Wu S. Quantitative assay by flow cytometry of the mitochondrial membrane potential in intact cells. Biochim Biophys Acta. 1998; 1404:393–404. [PubMed: 9739168]

Santangelo GM. Glucose signaling in *Saccharomyces cerevisiae*. Microbiol Mol Biol Rev. 2006; 70:253–282. [PubMed: 16524925]

Schedin S, Sindelar PJ, Pentchev P, Brunk U, Dallner G. Peroxisomal impairment in Niemann-Pick type C disease. J Biol Chem. 1997; 272:6245–6251. [PubMed: 9045641]

Shen D, Wang X, Li X, Zhang X, Yao Z, Dibble S, Dong XP, Yu T, Lieberman AP, Showalter HD, Xu H. Lipid storage disorders block lysosomal trafficking by inhibiting a TRP channel and lysosomal calcium release. Nat Commun. 2012; 3:731. [PubMed: 22415822]

Shimobayashi M, Oppliger W, Moes S, Jeno P, Hall MN. TORC1-regulated protein kinase Npr1 phosphorylates Orm to stimulate complex sphingolipid synthesis. Mol Biol Cell. 2013; 24:870–881. [PubMed: 23363605]

Sleat DE, Wiseman JA, El-Banna M, Price SM, Verot L, Shen MM, Tint GS, Vanier MT, Walkley SU, Lobel P. Genetic evidence for nonredundant functional cooperativity between NPC1 and NPC2 in lipid transport. Proc Natl Acad Sci U S A. 2004; 101:5886–5891. [PubMed: 15071184]

Sun Y, Miao Y, Yamane Y, Zhang C, Shokat KM, Takematsu H, Kozutsumi Y, Drubin DG. Orm protein phosphoregulation mediates transient sphingolipid biosynthesis response to heat stress via the Pkh-Ypk and Cdc55-PP2A pathways. Mol Biol Cell. 2012; 23:2388–2398. [PubMed: 22535525]

Tietze F. Enzymic method for quantitative determination of nanogram amounts of total and oxidized glutathione: applications to mammalian blood and other tissues. Anal Biochem. 1969; 27:502–522. [PubMed: 4388022]

Urban J, Soulard A, Huber A, Lippman S, Mukhopadhyay D, Deloche O, Wanke V, Anrather D, Ammerer G, Riezman H, Broach JR, De Virgilio C, Hall MN, Loewith R. Sch9 is a major target of TORC1 in *Saccharomyces cerevisiae*. Mol Cell. 2007; 26:663–674. [PubMed: 17560372]

Vanier MT. Lipid Changes in Niemann-Pick Disease Type C Brain: Personal Experience and Review of the Literature. Neurochemical Research. 1999; 24:481–489. [PubMed: 10227680]

Vanier MT. Niemann-Pick disease type C. Orphanet J Rare Dis. 2010; 5:16. [PubMed: 20525256]

Vanier MT, Millat G. Structure and function of the NPC2 protein. Biochim Biophys Acta. 2004; 1685:14–21. [PubMed: 15465422]

Vazquez MC, Balboa E, Alvarez AR, Zanlungo S. Oxidative stress: a pathogenic mechanism for Niemann-Pick type C disease. Oxid Med Cell Longev. 2012; 2012:205713. [PubMed: 22720116]

Vazquez MC, del Pozo T, Robledo FA, Carrasco G, Pavez L, Olivares F, Gonzalez M, Zanlungo S. Alteration of gene expression profile in Niemann-Pick type C mice correlates with tissue damage and oxidative stress. PLoS One. 2011; 6:e28777. [PubMed: 22216111]

Voordeckers K, Kimpe M, Haesendonckx S, Louwet W, Versele M, Thevelein JM. Yeast 3-phosphoinositide-dependent protein kinase-1 (PDK1) orthologs Pkh1–3 differentially regulate phosphorylation of protein kinase A (PKA) and the protein kinase B (PKB)/S6K ortholog Sch9. J Biol Chem. 2011; 286:22017–22027. [PubMed: 21531713]

Walkley SU, Suzuki K. Consequences of NPC1 and NPC2 loss of function in mammalian neurons. Biochim Biophys Acta. 2004; 1685:48–62. [PubMed: 15465426]

Wraith JE, Imrie J. New therapies in the management of Niemann-Pick type C disease: clinical utility of miglustat. Ther Clin Risk Manag. 2009; 5:877–887. [PubMed: 19956552]

Wu Z, Liu SQ, Huang D. Dietary restriction depends on nutrient composition to extend chronological lifespan in budding yeast *Saccharomyces cerevisiae*. PLoS One. 2013; 8:e64448. [PubMed: 23691220]

Xu M, Liu K, Swaroop M, Porter FD, Sidhu R, Finkes S, Ory DS, Marugan JJ, Xiao J, Southall N, Pavan WJ, Davidson C, Walkley SU, Remaley AT, Baxa U, Sun W, McKew JC, Austin CP, Zheng W. delta-Tocopherol reduces lipid accumulation in Niemann-Pick type C1 and Wolman cholesterol storage disorders. J Biol Chem. 2012; 287:39349–39360. [PubMed: 23035117]

Yu W, Gong JS, Ko M, Garver WS, Yanagisawa K, Michikawa M. Altered cholesterol metabolism in Niemann-Pick type C1 mouse brains affects mitochondrial function. J Biol Chem. 2005; 280:11731–11739. [PubMed: 15644330]

Zampieri S, Mellon SH, Butters TD, Nevyjel M, Covey DF, Bembi B, Dardis A. Oxidative stress in NPC1 deficient cells: protective effect of allopregnanolone. J Cell Mol Med. 2009; 13:3786–3796. [PubMed: 18774957]

Zhang S, Ren J, Li H, Zhang Q, Armstrong JS, Munn AL, Yang H. Ncr1p, the yeast ortholog of mammalian Niemann Pick C1 protein, is dispensable for endocytic transport. Traffic. 2004; 5:1017–1030. [PubMed: 15522102]

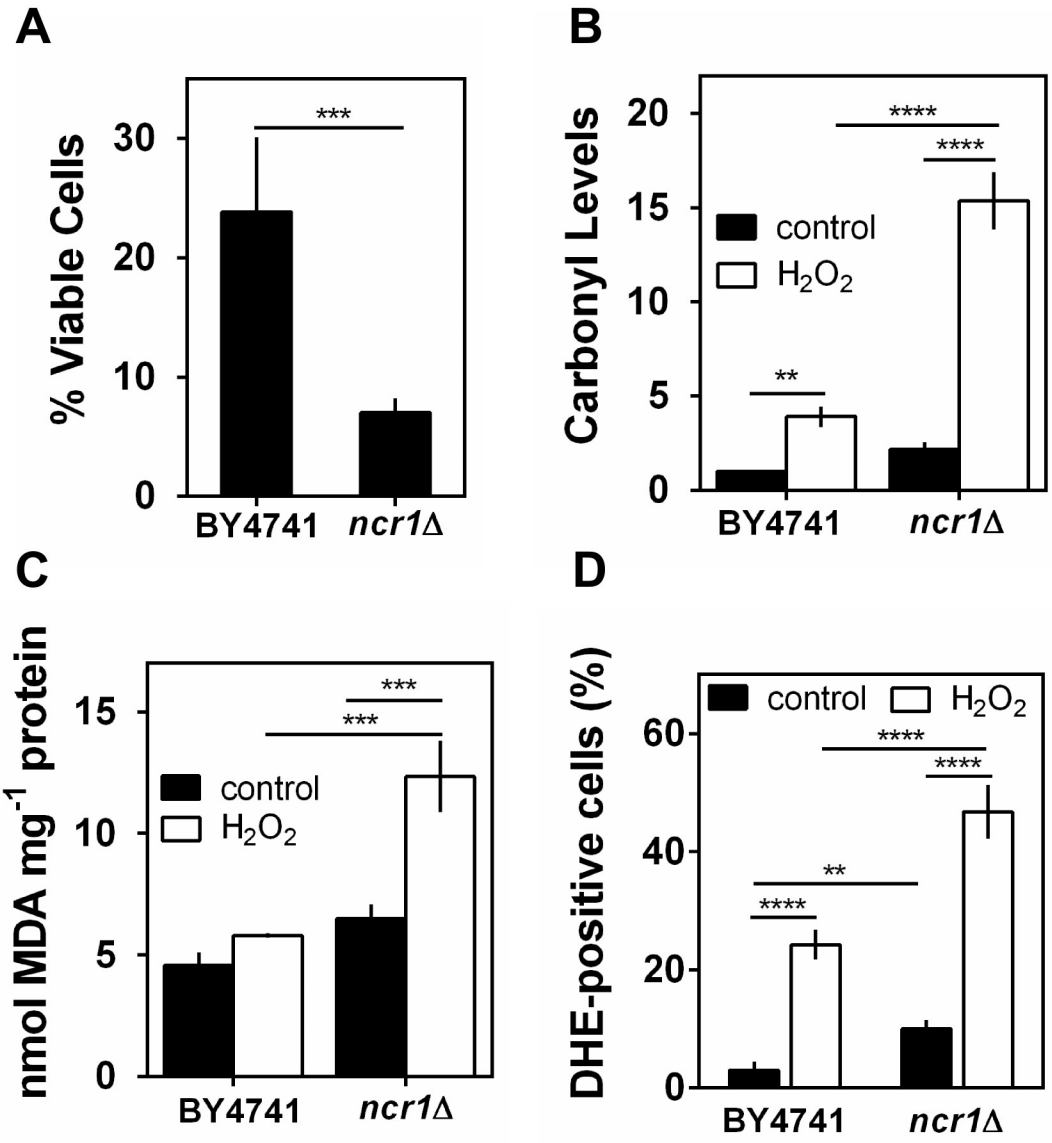

Fig. 1. Role of Ncr1p in hydrogen peroxide resistance

S. cerevisiae BY4741 and *ncr1*Δ::*KanMX4* cells were grown in SC-glucose medium to exponential phase ($O.D._{600nm}$=0.6) exposed to 1.5 mM H_2O_2 for 1 hour.

A. Cellular viability was measured as the percentage of the colony-forming unit (treated cells vs non-stressed cells). Values are mean ± SD of at least three independent experiments. ***p<0.001, unpaired Student's t-test.

B. Protein carbonylation. Proteins were derivatized with DNPH and slot-blotted into a PVDF membrane. Immunodetection was performed using an anti-DNP antibody. Quantitative analysis of total protein carbonyl content was performed by densitometry using data taken from the same membrane. Values are mean ± SD of at least three independent experiments.****p<0.0001, **p<0.01; Two-way ANOVA and Bonferroni test.

C. Lipid peroxidation. Cellular extracts were prepared and TBARS quantification was performed as described in Experimental procedures. Values are mean ± SD of at least three independent experiments. ***p<0.001; Two-way ANOVA and Bonferroni test.

D. Intracellular levels of superoxide radicals were analyzed by flow cytometry, using DHE as probe. Values are mean ± SD of at least three independent experiments. ****$p<0.0001$, **$p<0.01$; Two-way ANOVA and Bonferroni test.

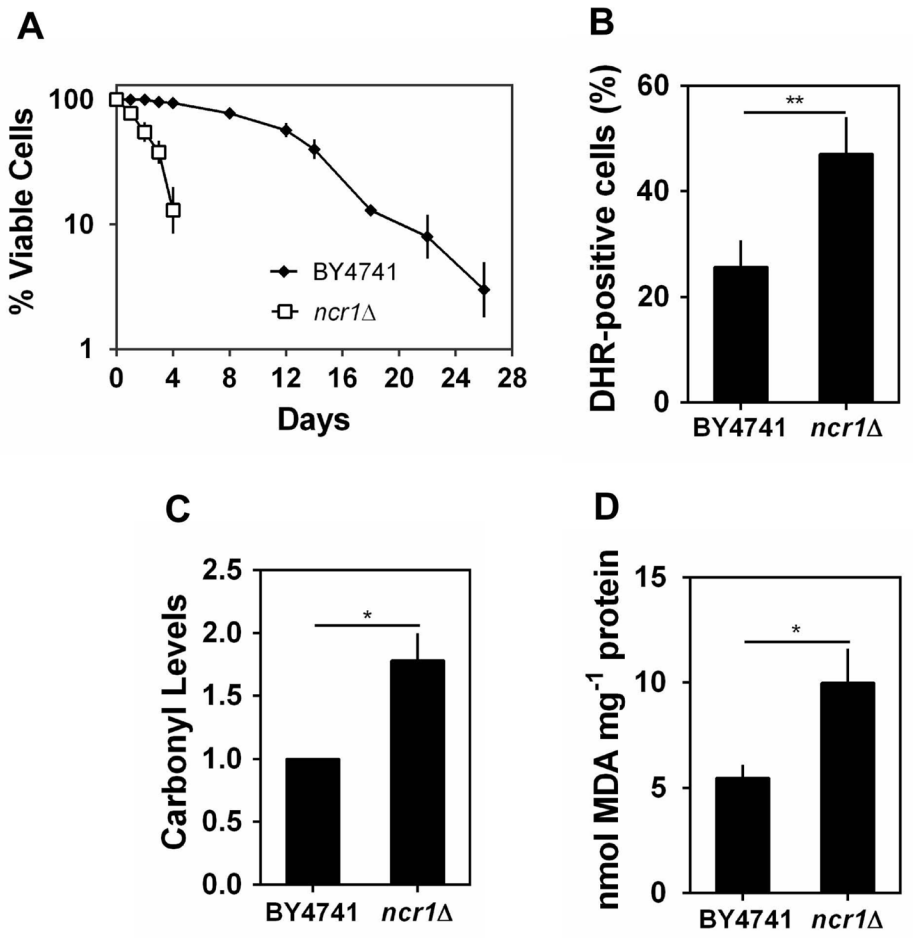

Fig. 2. Ncr1p deficiency decreases chronological lifespan

S. cerevisiae BY4741 and *ncr1*Δ::*KanMX4* cells were grown in SC-glucose medium at 26 ºC to PDS phase.

A. Cells were maintained in the growth medium overtime. Cellular viability was measured at 2 to 3 days intervals and was expressed as % colony forming units (aged vs day 0). Values are mean ± SD of at least three independent experiments.

B. Intracellular levels of hydrogen peroxide were analyzed by flow cytometry, using DHR 123 as probe. ***p*<0.01, unpaired Student's t-test.

C,D. Protein carbonylation and lipid peroxidation were measured as in Fig. 1B,C. Values are mean ± SD of at least three independent experiments. **p*<0.05, unpaired Student's t-test.

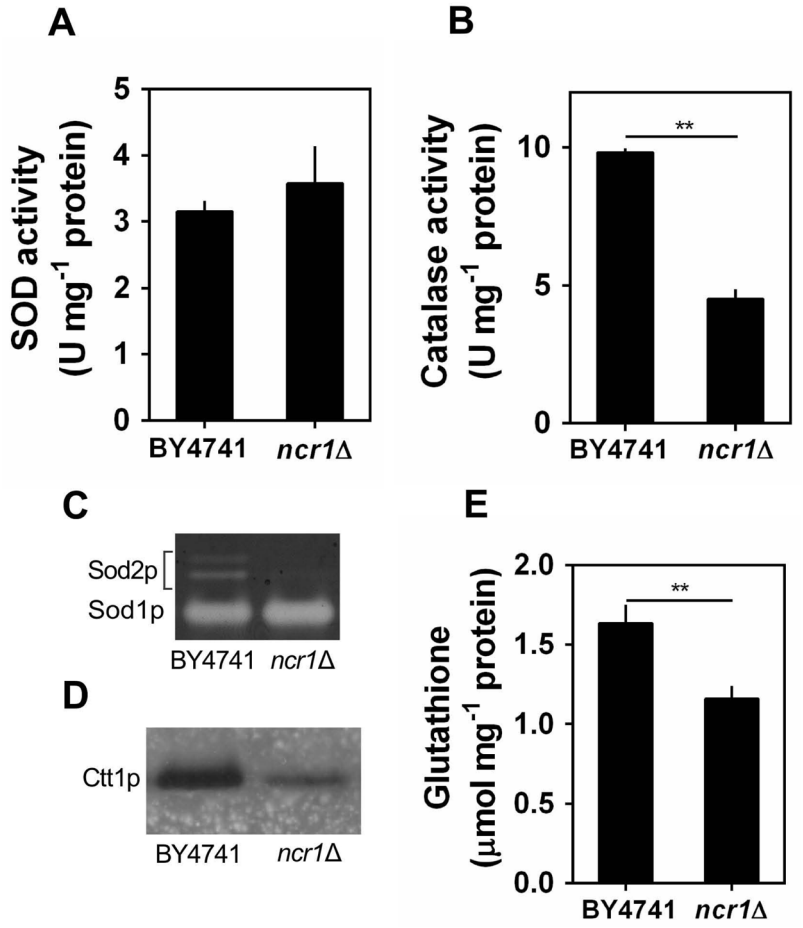

Fig. 3. Cytosolic catalase activity, mitochondrial superoxide dismutase activity and glutathione levels are decreased in *ncr1*Δ mutant cells

S. cerevisiae BY4741 and *ncr1*Δ::*KanMX4* cells were grown in SC-glucose medium to PDS phase.

A,B. The activity of superoxide dismutase (SOD) and catalase was measured spectrophotometrically. Values are mean ± SD of at least three independent experiments. ***p*<0.01, unpaired Student's t-test.

C,D. The activity of superoxide dismutases (Sod1p and Sod2p) or cytosolic catalase (Ctt1p) was assessed in situ after native-PAGE. One representative experiment out of three is shown.

E. Total glutathione levels. Reduced (GSH) + oxidized (GSSG) glutathione was measured as described in methods. Values are mean ± SD of at least three independent experiments. ***p*<0.01, unpaired Student's t-test.

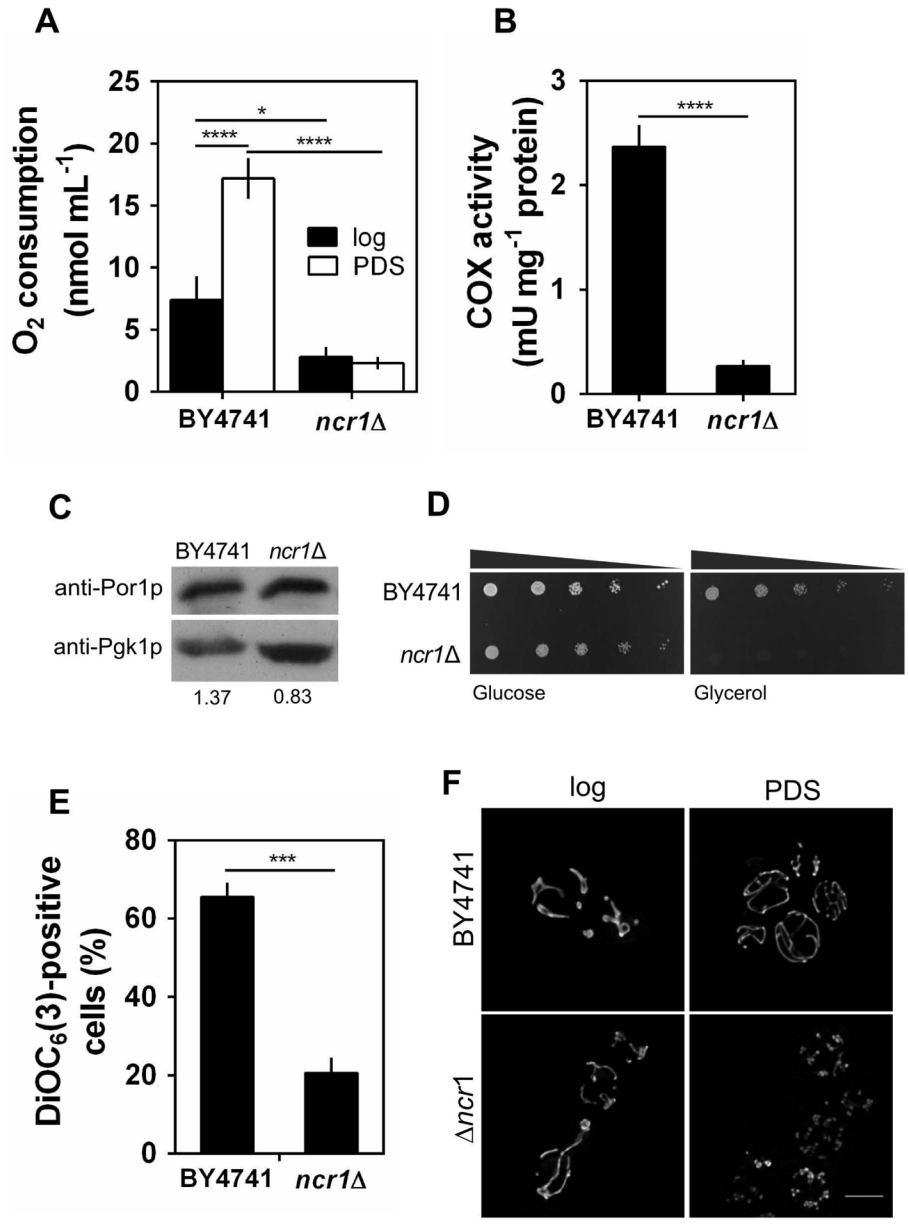

Fig. 4. Ncr1p deficiency decreases mitochondrial function and dynamics

S. cerevisiae BY4741 and *ncr1*Δ::*KanMX4* cells were grown in SC-glucose medium.

A. Oxygen consumption rates were measured in exponential (log) and PDS phase cells. Values are mean ± SD of at least three independent experiments. ****p<0.0001, *p<0.05; Two-way ANOVA and Bonferroni test.

B. Cytochrome *c* oxidase (COX) specific-activity was measured in cells grown to PDS phase. Values are mean ± SD of at least three independent experiments. ****p<0.0001, unpaired Student's t-test.

C. Immunoblot analysis of mitochondrial porin levels in cells grown to PDS phase. For each lane the Por1p signal was normalized to the signal for the Pgk1p internal standard (value shown below each lane). A representative experiment out of three is shown.

D. Cells were grown to exponential phase and fivefold serial dilutions were plated in solid medium containing glucose or glycerol as carbon source. One representative experiment out of three is shown.

E. Mitochondrial membrane potential was determined by flow cytometry using cells grown to PDS phase, unlabeled (auto fluorescence) or labeled with $DiOC_6(3)$. Representative histograms for each condition are shown in Supplemental Fig. S3. Values are mean ± SD of three independent experiments. ***$p<0.001$, unpaired Student's t-test.

F. *S. cerevisiae* BY4741 and *ncr1*Δ::*KanMX4* cells transformed with pYX222-mtDsRed (expressing mitochondrial DsRed) were grown to exponential (log) and PDS phase. Live cells were visualized by fluorescence microscopy. One representative experiment out of three is shown. Scale bar: 5 μm.

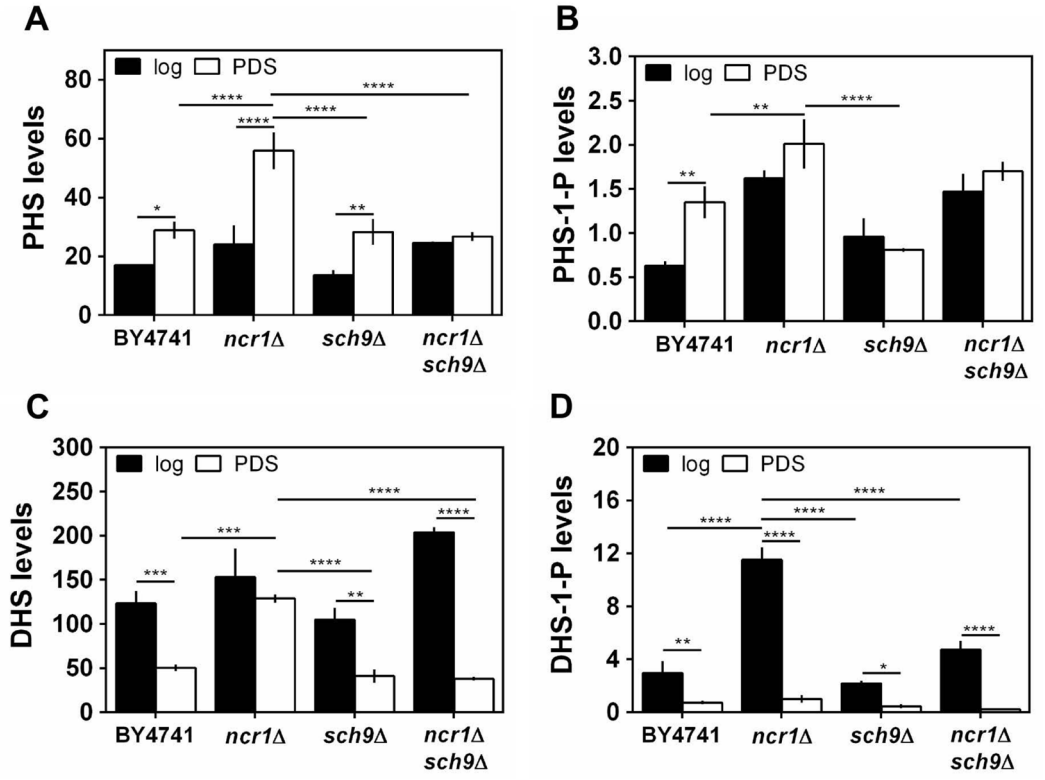

Fig. 5. Levels of long-chain sphingoid bases

S. cerevisiae BY4741, *ncr1*Δ::*URA3*, *sch9*Δ and *ncr1*Δ*sch9*Δ cells were grown in SC-glucose medium to the exponential (log) and post-diauxic shift (PDS) phase. Levels of indicated long chain bases were measured by HPLC-MS/MS. A. PHS - phytosphingosine; B. PHS-1-P – phytosphingosine-1-phosphate; C. DHS– dihydrosphingosine; D. DHS-1-P – dihydrosphingosine-1-phosphate. Data are expressed as pmol of lipid per total cell number (1.9×10^9) and are mean ± SD of three independent experiments. ****p<0.0001, ***p<0.001, **p<0.01, *p<0.05; Two-way ANOVA and Bonferroni test.

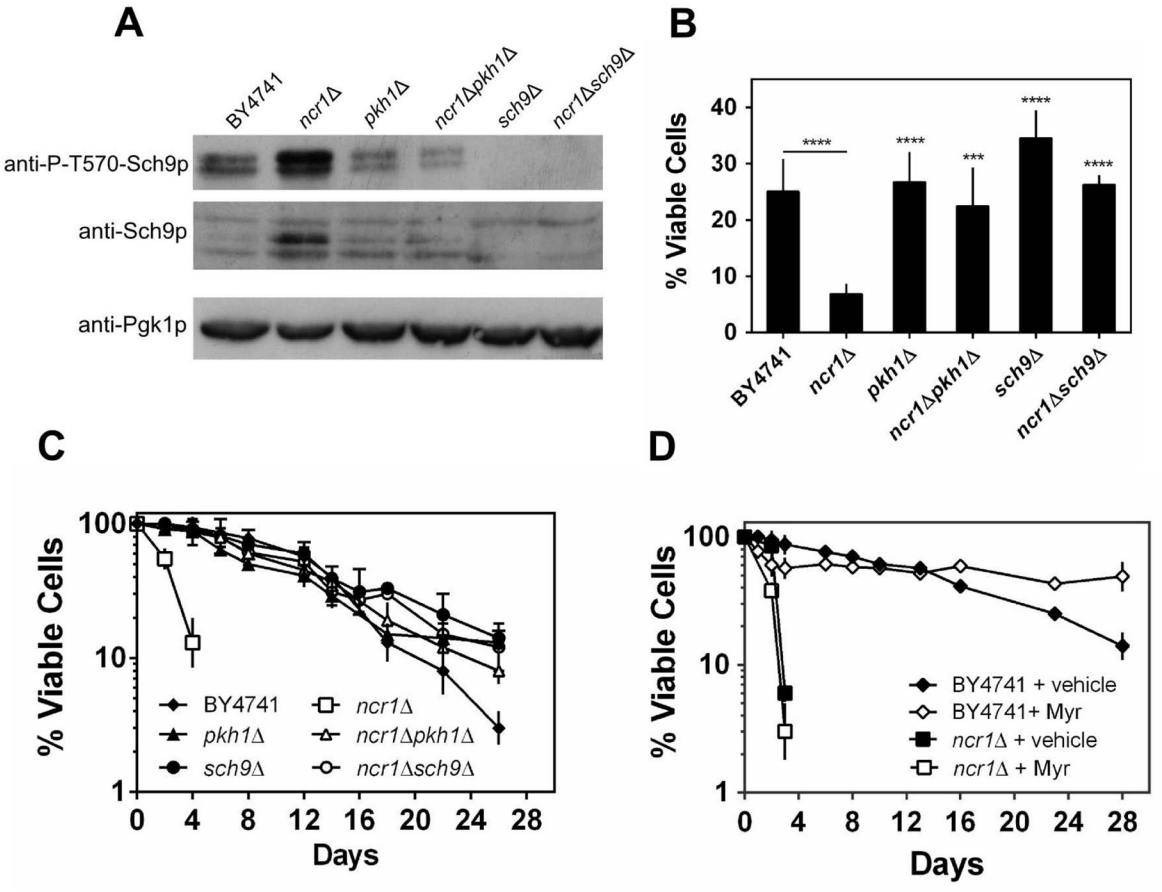

Fig. 6. Ncr1p deficient cells exhibit increased levels of Sch9p and Sch9p-phospho-T570 and *ncr1*Δ phenotypes are suppressed by disruption of *PKH1* or *SCH9* but not by myriocin

S. cerevisiae BY4741, *ncr1*Δ::*URA3*, *pkh1*Δ, *ncr1*Δ*pkh1*Δ, *sch9*Δ and *ncr1*Δ*sch9*Δ cells were grown in SC-glucose medium to exponential (A and B) or PDS (C and D) phase.

A. Immunoblot analysis of Sch9p and P-T570-Sch9p. Pgk1p was used as loading control. . A representative experiment out of three is shown.

B,C. Hydrogen peroxide resistance (B) and chronological lifespan (C) were measured as in Fig. 1A and 2A, respectively. Values are mean ± SD of at least three independent experiments. ****p<0.0001, ***p<0.001 (relative to *ncr1*Δ); Two-way ANOVA and Bonferroni test.

D. Analysis of chronological lifespan in *S. cerevisiae* BY4741 and *ncr1*Δ::*KanMX4* cells treated with ethanol (vehicle) or myriocin (600 ng mL^{-1}; Myr). Values are mean ± SD of at least two independent experiments.

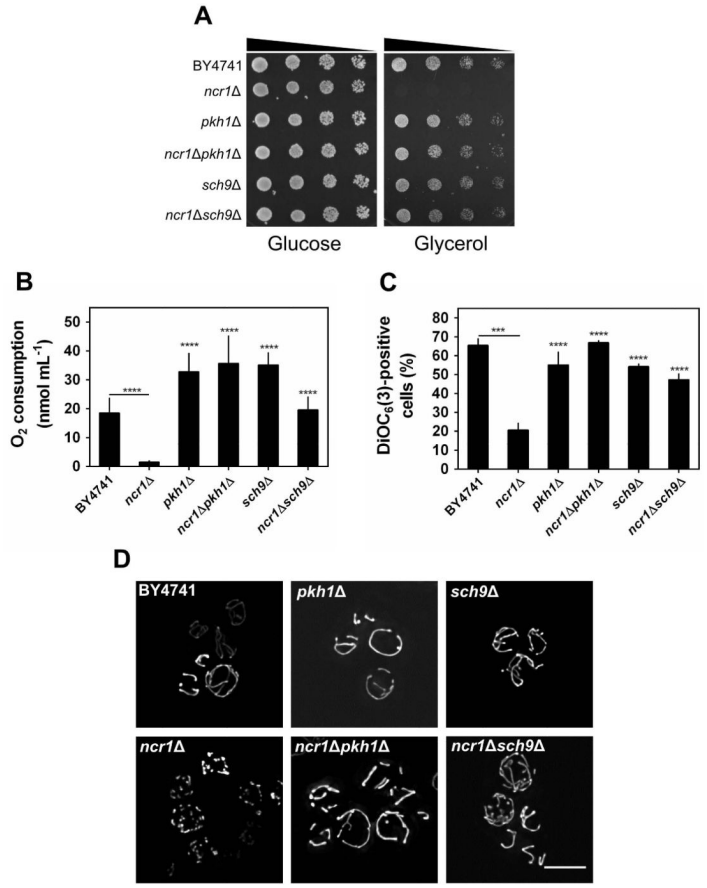

Fig. 7. Role of the LCB→Pkh1p→Sch9p pathway in mitochondrial dysfunction of *ncr1*Δ cells

S. cerevisiae BY4741, *ncr1*Δ::*URA3*, *pkh1*Δ, *ncr1*Δ*pkh1*Δ, *sch9* and *ncr1*Δ*sch9*Δ cells were grown in SC-glucose medium.

A. Cells were grown to exponential phase and fivefold serial dilutions were plated in solid medium containing glucose or glycerol as carbon source. One representative experiment out of three is shown.

B. Oxygen consumption rates were measured in PDS phase cells. Values are mean ± SD of at least three independent experiments. ****$p<0.0001$ (relative to *ncr1*Δ); Two-way ANOVA and Bonferroni test.

C. Mitochondrial membrane potential was determined by flow cytometry using PDS phase cells, unlabeled (auto fluorescence) or labeled with $DiOC_6(3)$. Values are mean ± SD of three independent experiments. ****$p<0.0001$, ***$p<0.001$ (relative to *ncr1*Δ); Two-way ANOVA and Bonferroni test.

D. *S. cerevisiae* cells transformed with pYX222-mtDsRed (expressing mitochondrial DsRed) were grown to PDS phase. Live cells were visualized by fluorescence microscopy. One representative experiment out of three is shown. Scale bar: 5 μm.

Table 1

S. cerevisiae strains used in this work.

Strain	Genotype	Reference/Source
BY4741[*,¥]	Mata, *his3*Δ1, *leu2*Δ0, *met15*Δ0, *ura3*Δ0	EUROSCARF
*ncr1*Δ::*KanMX4*[*,¥]	BY4741 *ncr1*Δ::*KanMX4*	This study
*ncr1*Δ::*URA3*	BY4741 *ncr1*Δ::*URA3*	This study
*sch9*Δ[*]	BY4741 *sch9*D::*KanMX4*	EUROSCARF
*ncr1*Δ*sch9*Δ[*]	BY4741 *ncr1*Δ::*URA3 sch9*Δ::*KanMX4*	This study
*pkh1*Δ[*]	BY4741 *pkh1*Δ::*KanMX4*	EUROSCARF
*ncr1*Δ*pkh1*Δ[*]	BY4741 *ncr1*Δ::*URA3 pkh1*Δ::*KanMX4*	This study

[*] Cells harboring pYX222-mtDsRed are indicated.

[¥] Cells harboring YEp352, YEp352-*SOD2* and YEp352-*CTT1* are indicated.